RESEARCH ARTICLE
PLANETARY SCIENCES

Earth and Planetary Physics
10: 196–204, 2026
doi: 10.26464/epp2025080

Taxonomic classification of 80 near-Earth asteroids

Fan Mo[1,2], Bin Li[1,2*], HaiBin Zhao[1*], Jian Chen[1,2], Yan Jin[3], MengHui Tang[3], Igor Molotov[4], A.M. Abdelaziz[5], A. Takey[5], S.K. Tealib[5], Ahmed. Shokry[5], and JianYang Li[6]

[1]Purple Mountain Observatory, Chinese Academy of Sciences, Nanjing 210023, China;

[2]School of Astronomy and Space Sciences, University of Science and Technology of China, Hefei 230026, China;

[3]Earth Observation System and Data Center, China National Space Administration, Beijing 100101, China;

[4]Keldysh Institute of Applied Mathematics, Russian Academy of Sciences, Miusskaya sq. 4, Moscow, 125047, Russia;

[5]National Research Institute of Astronomy and Geophysics (NRIAG), Helwan, Cairo 11421, Egypt;

[6]Planetary Environmental and Astrobiological Research Laboratory (PEARL), School of Atmospheric Sciences, Sun Yat-sen University, Zhuhai 510275, China

Key Points:

- A number of multicolor observations of near-Earth asteroids (NEAs) are presented.
- The taxonomic classification of observed near-Earth asteroids (NEAs) are analyzed.
- The distribution of NEAs by taxonomy is discussed.

Citation: Mo, F., Li, B., Zhao, H. B., Chen, J., Jin, Y., Tang, M. H., Molotov, I., Abdelaziz, A. M., Takey, A., ... Li, J. Y. (2026). Taxonomic classification of 80 near-Earth asteroids. *Earth Planet. Phys.*, *10*(1), 196–204. http://doi.org/10.26464/epp2025080

Abstract: Near-Earth objects are important not only in studying the early formation of the Solar System, but also because they pose a serious hazard to humanity when they make close approaches to the Earth. Study of their physical properties can provide useful information on their origin, evolution, and hazard to human beings. However, it remains challenging to investigate small, newly discovered, near-Earth objects because of our limited observational window. This investigation seeks to determine the visible colors of near-Earth asteroids (NEAs) , perform an initial taxonomic classification based on visible colors and analyze possible correlations between the distribution of taxonomic classification and asteroid size or orbital parameters. Observations were performed in the broadband BVRI Johnson–Cousins photometric system, applied to images from the Yaoan High Precision Telescope and the 1.88 m telescope at the Kottamia Astronomical Observatory. We present new photometric observations of 84 near-Earth asteroids, and classify 80 of them taxonomically, based on their photometric colors. We find that nearly half (46.3%) of the objects in our sample can be classified as S-complex, 26.3% as C-complex, 6% as D-complex, and 15.0% as X-complex; the remaining belong to the A- or V-types. Additionally, we identify three P-type NEAs in our sample, according to the Tholen scheme. The fractional abundances of the C/X-complex members with absolute magnitude $H \geq 17.0$ were more than twice as large as those with $H < 17.0$. However, the fractions of C- and S-complex members with diameters ≤1 km and >1 km are nearly equal, while X-complex members tend to have sub-kilometer diameters. In our sample, the C/D-complex objects are predominant among those with a Jovian Tisserand parameter of $T_J < 3.1$. These bodies could have a cometary origin. C- and S-complex members account for a considerable proportion of the asteroids that are potentially hazardous.

Keywords: near-Earth asteroids; optical telescope; photometric observation; taxonomic classification

1. Introduction

The near-Earth asteroids (NEAs) are a subgroup of asteroids whose orbits intersect with the Earth's. Study of NEAs is important for both planetary science and planetary defense; it can answer such interesting scientific questions as how our Solar system formed and evolved, including how planets formed and how the early Earth acquired water and organics. The Chelyabinsk event in 2013 drew widespread attention to what more needs to be done to detect asteroids of its size (or larger) before they strike our planet. The Double Asteroid Redirection Test (DART) mission successfully changed the orbital period of Dimorphos (Thomas et al., 2023) and demonstrated the kinetic-impact technique for nudging an asteroid off a predicted impact course with Earth. Additionally, the discovery of objects like 2016 HO_3, which has a stable orbit around Earth and is considered a potential target for deep-space exploration (Zhang T et al., 2021), underscores the need for accurate characterization of NEAs for both planetary defense and space exploration purposes.

Classification of NEAs according to their spectra has been an effective tool. In the case of NEAs, characteristics such as surface composition, origin, and evolution appear to be promising classificatory variables that will elucidate their histories. Based on the

First author: F. Mo, fanmo@pmo.ac.cn
Correspondence to: B. Li, binli@pmo.ac.cn
H. B. Zhao, meteorzh@pmo.ac.cn
Received 08 MAY 2024; Accepted 30 MAY 2025.
First Published online 25 JUL 2025.

features in ultraviolet (UV) to near infrared (NIR) wavelength reflectance spectra, together with albedo and photometric color indices, the most common spectral taxonomies currently in use are the Tholen (Tholen, 1984), Bus (Bus and Binzel, 2002), and Bus-DeMeo (DeMeo et al., 2009) schemes. Asteroid spectra are traditionally divided into three major complexes: C-, S- and X-complex. The C-complex NEAs have featureless spectra with flat or low slopes and are of special interest because of their volatile contents (Nichols, 1993; Reddy et al., 2012). The S-complex NEAs are characterized by spectra with moderate silicate absorption features at 1 and 2 μm, whose spectral properties are similar with ordinary chondrites (Vernazza et al., 2008). At the same time, the mismatch between the distribution of S-type NEAs and ordinary chondrites has inspired discussion of the mechanisms of space weathering (Vernazza et al., 2009) and surface reconstruction (Binzel et al., 2010). The X-complex NEAs can be further classified into E/M/P types based on high/medium/low albedo.

The diverse taxonomic types in near-Earth population match the diversity of the main-belt, with all main-belt taxonomic classes represented (Binzel et al., 2019), but the abundance of A-type and D-type is higher among small NEAs (Perna et al., 2018). The taxonomic spectral distribution is strongly associated with orbital parameters such as perihelion distance; Q-type NEAs typically have lower perihelion distance and larger size, which may be related to surface renewal due to thermal fatigue (Binzel et al., 2019, Popescu et al., 2019). NEAs of different spectral types show significant differences in composition and space weathering effects. C-complex and D-type NEAs with low albedos show limited space weathering, while S-complex and A-type NEAs with medium and high albedos show strong space weathering effects (Perna et al., 2018). The taxonomic distribution of potentially hazardous asteroids (PHAs) is similar to that of overall NEA population, with Q/S-types and V-types dominating (Binzel et al., 2019, Popescu et al., 2019).

Although spectroscopic surveys allow for more accurate classification of NEAs, photometric surveys have the advantage of lower observation requirements, higher observation efficiency, and the ability to observe fainter objects. Over recent decades, several photometric surveys have been conducted and the taxonomic distribution of NEAs has been subjected to more detailed analysis. Ye QZ (2011) and Lin CH et al. (2018) both found that the fraction of C-cluster NEAs (including those in the C- and X-complexes) is larger within smaller NEAs (those with absolute magnitude H > 17.0). However, considering the average albedos of each complex, the C-complex NEAs seem to be slightly underrepresented below diameter <400 m (Ieva et al., 2020). Therefore, the distribution of C-complex NEAs according to size deserves more study because of their low albedo and likely observational bias.

The taxonomic distribution of NEAs according to orbital parameters is always linked with their source region. Ieva et al. (2020) confirmed that the S-complex NEAs show a lower median value for semi-major axis, a, and perihelion, q, when compared to those in the C-complex. It has also been found that NEAs with low-Jovian Tisserand parameter (T_J < 3) are dominated by carbonaceous objects, which could be extinct or dormant comets (Hromakina et al., 2021). Additionally, thanks to the several sky surveys—for example, the Sloan Digital Sky Survey (SDSS), it is possible to classify a large number of asteroids (e.g. Szabó et al., 2004; Hasselmann et al., 2015; Sergeyev and Carry, 2021; Roh et al., 2022). Although significant progress has been made in taxonomic classification of NEAs, the number that have been classified still accounts for less than 10% of the total observed population (Popescu et al., 2019). Moreover, due to their low brightness, sub-kilometer NEAs have been relatively neglected and urgently require more attention.

In this paper, we present photometric color indices and a taxonomic classification of a sample of 80 objects. Below, in Section 2 we describe our observational strategy and data reduction procedures; in Section 3 we present our taxonomic classification of the observed objects by spectral characteristics, and our statistical analysis of the results; in Section 4, we discuss the results; in Section 5 we present our conclusions.

2. Observations and Data Reduction

The data presented in this work were collected between October 2023 and October 2024 at the Purple Mountain Observatory Yaoan High Precision Telescope (YAHPT, IAU code O49) in China and the Kottamia Astronomical Observatory 1.88 m telescope (IAU code 088) in Egypt.

The CCD camera installed on YAHPT is a PI CCD camera which has a field of view (FOV) of 11.8′ × 11.8′ and an effective pixel scale of 0.347″/pxl; the recording device on the 1.88 m telescope is a Kottamia Faint Imaging Spectro-Polarimeter (KFISP) with FOV of 8′ × 8′ and a pixel scale of 0.25″/pxl (Azzam et al., 2022). The filters used at both telescope locations are Johnson broad-band BVRI filters with central wavelengths at 440, 550, 710 and 790 nm.

For KFISP, we adopted the star-focusing observational mode. Our observational strategy for YAHPT, however, was to adopt the moving object tracking observational mode, which allows for longer exposure times to observe faint objects. Also, to detect targets moving fast and star trails longer than 10″, we added observations of stars with similar air mass, which is a measure of the amount of air along the line of sight when observing a star or other celestial source from below Earth's atmosphere, in order to obtain accurate photometry of reference stars.

We selected the targets using the Observation Planning Tool available from the ESA's Near-Earth Object Coordination Centre (https://neo.ssa.esa.int/neo-toolkit) and the NEA Observation Planning Aid at the IAU's Minor Planet Center (https://www.minorplanetcenter.net/cgi-bin/neaobs.cgi). For YAHPT, we selected NEAs with visible magnitude brighter than 19.0 mag, while for KFISP we selected NEAs with visible magnitude brighter than 18.5 mag and proper motion lower than 3″/min. All observations were conducted with the color sequence as BVBVRVRIRI in order to reduce the color error caused by an NEA's rotation. We adjusted the exposure time to obtain a signal-to-noise ratio of at least 30 in VRI filters and at least 10 in the B filter. The photometric error in VRI filters is less than 0.1 mag and in B filter less than 0.15 mag. The observational log can be found in Table S1.

Images were reduced following the standard procedure: bias subtraction and flat field correction; background reduction and

source extraction using python package SEP (Barbary, 2016); measurement of instrumental magnitude via Kron aperture photometry (Kron, 1980); World Coordinate Systems information application with the code from astrometry.net (Lang D et al., 2010); target position from Astroquery.MPC (Ginsburg et al., 2019). Absolute calibration was carried out using field stars from the Pan-STARRS catalog because it provides the Kron magnitude used in this work. As the magnitudes in the Pan-STARRS1 catalog are provided in the Sloan photometric system, we used the transformation to the Johnson-Cousins system from Tonry et al. (2012). Besides, the reference stars we chose not only had better S/N than targets, but also had Sun-like colors (i.e., B-V, V-R and R-I colors within 0.1 mag of the Sun). Finally, we derived the reduced magnitude of the target from each observation. The median S/N values of the B-band observations from YAHPT and KFISP are 18.65 and 25.05, while the median full width at half maximum are 8.42 and 6.97 pixels, respectively.

The color indices and their errors are computed according to the color sequence. Taking the color index B-V for example, we compute the mean value of reduced magnitude from the two B-band observation and obtain the B-V for the first time by subtracting the first V-band magnitude from the mean value of B-band photometry. Similarity, we obtain the B-V for the second time by subtracting the mean value of the first two V-band magnitude from the second B-band magnitude. Then, the final B-V is the mean value of these two B-Vs. The error is computed following standard error propagation. All the color indices used for our taxonomic classification are listed in Table S1.

3. Results and Data Analysis

In total, we reduced photometric measurements and computed color indices for a total sample of 84 individual NEAs. The taxonomic classification method is described as follows.

3.1 Taxonomic Classification

We classified the asteroids in our sample by calculating the distances between the reflectance transferred from color indices and the mean spectra of each type from DeMeo et al. (2009). We defined the distance between two spectral curves as Equation (1):

$$d_{ij} = \sqrt{\frac{1}{N}\sum_{k=1}^{N}\frac{\left(x_{ik}-x_{jk}\right)^2}{\sigma_{ik}^2+\sigma_{jk}^2}}, \tag{1}$$

where N is the number of data point, x_{ik}, σ_{ik}, x_{jk} and σ_{jk} are respectively the reflectance values and their standard deviations of the spectra i and j at the k^{th} data point.

First, we calculated the pairwise distances between the mean spectra of each type. Since the distribution of these distances exhibits a long tail, we set the median value instead of the mean value of them as the threshold for the taxonimic classification of NEAs, which can mitigate the influence of extreme values and constrain the classification more strictly. Then, starting from the B-V, V-R, and R-I color indices, we normalized to unity the reflectance at the V filter, and re-scaled the B, R, and I reflectance using Equation (2):

$$R_\lambda = 10^{-0.4[(M_\lambda - V)-(M_\lambda - V)_{\text{sun}}]}, \tag{2}$$

where $M_\lambda - V$ and $(M_\lambda - V)_{\text{sun}}$ are the colors for the object and the Sun at wavelength λ, respectively. Since we could obtain reflectance only at specific wavelengths, and the mean spectra of each type, spanning wavelengths from 0.45 to 2.45 μm, was sampled at intervals of 0.05 μm, we interpolated the mean spectra and resampled it at 0.01 μm intervals from 0.45 to 0.80 μm. Afterwards, we extrapolated the resampled mean spectra to 0.44 μm.

Following that, we calculated the distances between every set of reflectance data points obtained from color indices and the mean spectra of each class. Finally, for each set of reflectance data points, we found the corresponding type that has the minimum distance. If the minimum distance was less than the threshold we set earlier, we regarded the corresponding type as the target's taxonomy type. In contrast, if the minimum distance was greater than the threshold, we considered that the target's taxonomy type could be confirmed through our observational results and recorded the target as U-type. The results of this taxonomic classification of each observation record are listed in Table S1.

Although we recognize that our color indices cannot provide high-resolution data comparable to spectroscopic observations and are also restricted to the optical wavelength range, our goal is to facilitate a more robust statistical analysis by considering four major groups and several end members (DeMeo et al., 2009): the C-complex (including B-, C-, Cb-, Cgh-, and Ch- type objects), the D-complex (including D- and T-type objects), the S-complex (including K-, L-, Q-, S-, Sa-, Sq-, Sr-, and Sv-type objects) and the X-complex (including X, Xc-, Xe-. and Xk-type objects) and the end members (including A- and V-type objects). The Cg-, O-, R- and Xn-types are excluded from our classification because their mean spectra are provided without errorbar.

In Table S2, after excluding those classified as U-type, we provide the taxonomic classification for 80 NEAs: 37 asteroids are classified as belonging to the S-complex, 21 to the C-complex, 12 to the X-complex, and 5 to the D-complex, plus one A-type and four V-type. Normalized reflectance and mean spectra for each asteroid complex are presented in Figure 1. Specially, for those objects with multiple observations and different taxonomic classifications, we chose the result with less error and distance to the mean spectra of their spectral types.

Thirty-five objects in our sample had been classified previously; our work classifies 31 of these objects into the same taxonomy complex as they had been in the literature. Objects (3838) and (448818) had been classified as C-type and V-type, respectively, through multi-filter photometry in SDSS (Sergeyev and Carry, 2021), but are categorized here as S-complex and D-complex. Similarly, (11398) and (174050) were both classified as Sr-type in MITHNEOS (DeMeo et al., 2014; Marsset et al., 2022), yet are identified as D-complex and X-complex, respectively, in our analysis.

In Figure 2, we show the B-R versus V-I color–color diagram for objects classified in Table S2. The diagram clearly shows distinct regions occupied primarily by members of different taxonomic complexes, confirming the reliability of our classification. A general agreement for C-, D-, S-, and X-complex is evident. In Table 1, we present median B-R and V-I colors (along with their corresponding 1σ deviations) for the objects in our sample that

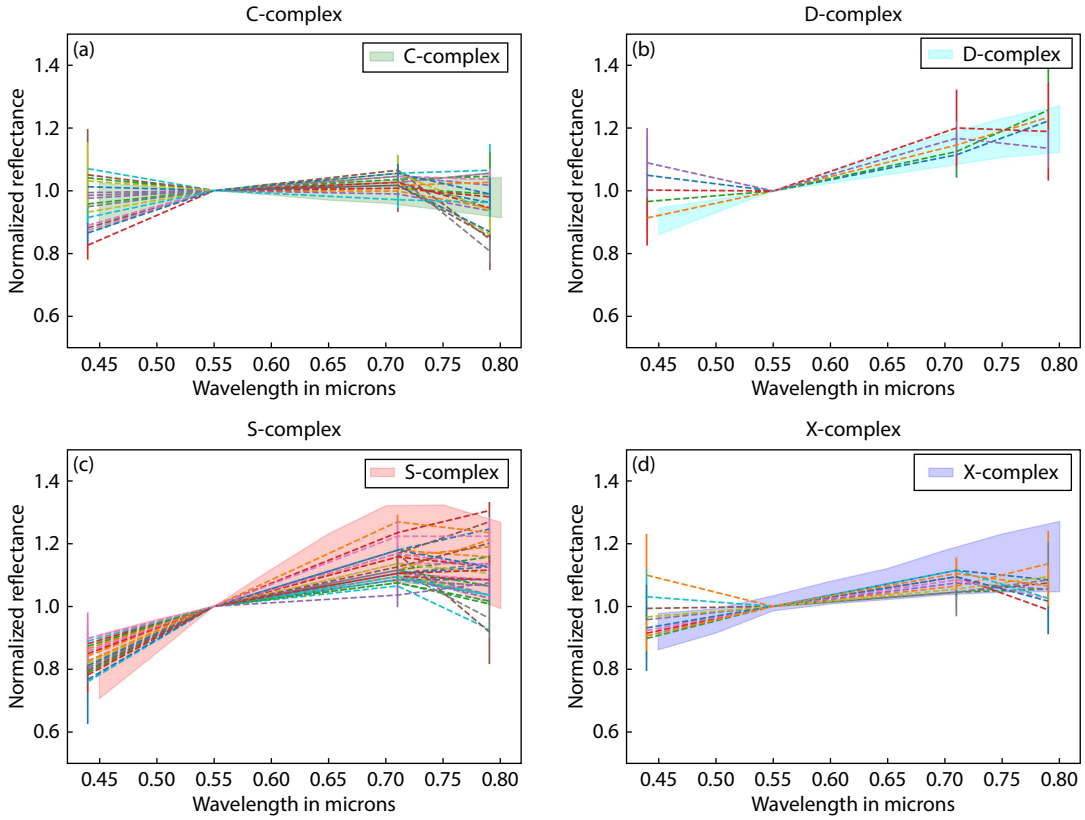

Figure 1. Normalized reflectance spectra of C- (a), D- (b), S- (c) and X-complex (d) NEAs in our sample.

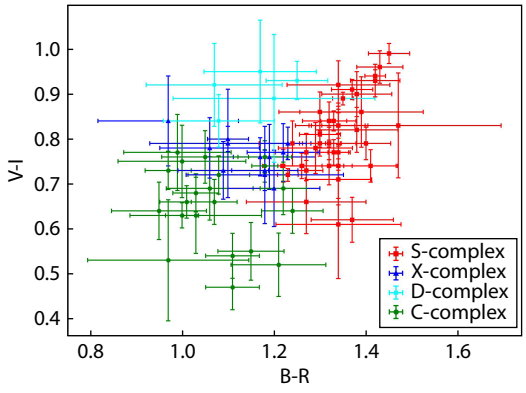

Figure 2. B-R v.s. the V-I color indices for the example.

Table 1. B-R and V-I color ranges found in our sample, using the DeMeo sample spectra.

	(B-R)*	$(B-R)_{DeMeo}$	(V-I)*	$(V-I)_{DeMeo}$
C	1.06 ± 0.09	$1.09^{+0.11}_{-0.09}$	0.66 ± 0.09	$0.69^{+0.04}_{-0.10}$
S	1.34 ± 0.06	$1.29^{+0.14}_{-0.11}$	0.79 ± 0.09	$0.82^{+0.10}_{-0.14}$
X	1.17 ± 0.07	$1.13^{+0.12}_{-0.07}$	0.77 ± 0.04	$0.78^{+0.06}_{-0.04}$

we assign to the C-, S-, and X-complexes, together with the DeMeo colors computed by Ieva et al. (2018). Also, for A- and V-type objects, we obtained the BR slope for each object: (414903) is classified as A-type with BR slope 20 ± 3.9%/100 nm, which is lower than the mean BR slope 25.1 ± 3.5%/100 nm of A-type objects in SMASS; the BR slope of V-type objects (137924, 163696, 439437 and 2024 CS6) in our sample are 21 ± 2.4%/100 nm, 13 ± 1.8%/100 nm, 12 ± 0.7%/100 nm and 12 ± 0.7%/100 nm, respectively, compared to the mean BR slope of V-type objects obtained by Ieva et al. (2016), 12.12 ± 6.4%/100 nm, which is consistent with three of our results.

3.2 Statistical Analysis

Since the numbers of A-, D- and V-types are relatively small, the following statistical analysis will focus on the C-, S- and X-complex asteroids.

The distribution of asteroids by taxonomic complexes presented in Figure 3. In order to look for possible differences in the distribution of the taxonomic complexes, we divided our sample into two nearly equal bins considering objects with the absolute magnitude $H \leq 17.0$ and those with $H > 17.0$. The NEAs with $H \leq 17$ appear to have a significantly higher proportion of S-complex objects. As for C- and X-complex objects, their abundances are higher among in smaller objects ($H > 17$). In detail, the C/X-complex abundance of large NEAs with $H \leq 17$ is 0.20, while the abundance of smaller ones (with $H > 17$) is 0.48.

The size of asteroid can be computed by absolute magnitude and albedo, following Equation (3) in Harris and Harris (1997):

$$\text{diamater} = 10^{-H/5} 1329/\sqrt{p_v}, \tag{3}$$

where p_v is albedo; diamater in km. However, albedo values are available for only about one-third of NEAs in our sample through infrared observations and thermal models (e.g. Mainzer et al.,

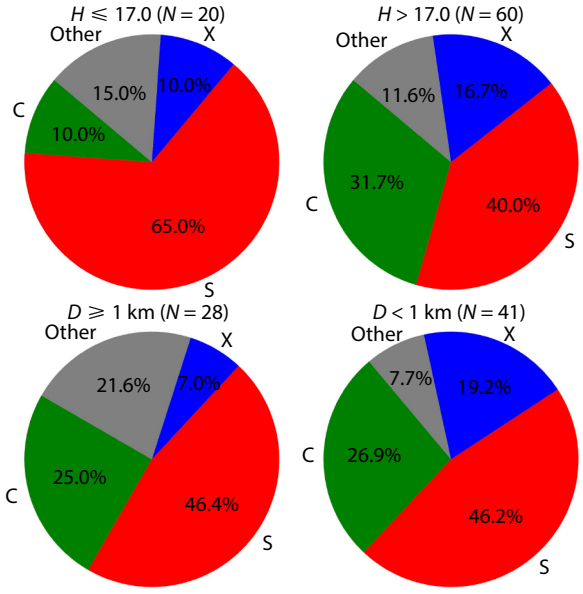

Figure 3. Distribution of the taxonomic complexes observed in our survey between different absolute magnitudes and different diameters.

2011). Therefore, to obtain the size of each observed NEA, if its actual albedo was not available, we used the *average* albedo of other members of its taxonomic complex. Thomas et al. (2011) gave the average albedo by taxonomic complex in the NEA population: 0.13 for C-complex, 0.02 for D-complex, 0.26 for S-complex, 0.42 for V-type and 0.31 for X-complex. Figure 3 shows the distribution of the taxonomic complexes in our sample between diameters $\geq$ 1 km and < 1 km, where diameter = 1 km roughly corresponds to H = 17, assuming an albedo of 0.26. We notice that the C- and S-complexes maintain a roughly constant fraction, fluctuating around the fraction of the whole sample, while the fraction of X-complex decreases steeply in the range of diameter $\geq$ 1 km.

As shown in Figure 3, the distributions of taxonomic complexes in our sample with respect to absolute magnitude and diameter exhibit significant discrepancies. These discrepancies are likely attributable to the varying albedos of asteroids belonging to different taxonomic classes. Specifically, C-complex asteroids, which possess lower albedos, appear fainter compared to asteroids of the same size from higher-albedo taxonomic classes, thereby shifting them into bins corresponding to higher absolute magnitudes. Additionally, the observational magnitude limit also implies that S-complex objects are easier to detect than C-complex objects of the same size.

In order to investigate the relationship between NEA's surface physical characteristics and dynamic properties, we analyzed the taxonomic distribution in our sample according to their orbital parameters: semi-major axis a, eccentricity e, inclination i, perihelion q, aphelion Q, minimum orbit intersection distance (MOID) and Jovian Tisserand parameter T_J. The median values and the median absolute deviations (MADs) of orbital elements for C-, S- and X-complex members are shown in Table 2. The X-complex objects have the highest median values for a, q and Q.

In Figure 4, we show the distribution of each complex in our sample among three different orbital types. The bar chart demonstrates a clear dominance of the S-complex in the Apollo and Amor groups and indicates that the X-complex exhibits a preference towards the Amor group, which is distinct from C- and S-complexes.

The Jovian Tisserand parameter T_J is a parameter designed to distinguish asteroids dynamically from comets (e.g. Kresák, 1972; Kosai, 1992). According to the Tancredi (2014) criterion, NEAs with T_J < 3.1 are considered as NEAs on cometary orbits (or NEACOs). Among the eleven NEACOs in our sample, there are seven primitive C/D-complex, two S-complex and two X-complex members.

Figure 5 shows the value of the Earth's MOID versus diameter. The vertical line at MOID = 0.05 au and the horizontal line at diameter = 140 m separate PHAs from the rest of the NEAs. It is interesting that there are no observed objects with small sizes (diameter <140 m) and large MOIDs (>0.05 au), a result that may be a manifestation of observation bias. All D-complex members have moderate MOIDs and small absolute magnitudes, which may be the result of a combination of their source region and low albedos. Among the 13 PHAs we classified, there are five C-complex, five S-complex, two X-complex and one V-type objects, which may require different planetary defense options because of their different material properties.

4. Discussion

Several factors may introduce errors that could affect our taxonomic classification. Although we have adopted an optimized color sequence in our observations, measurement errors of color indices due to the NEAs' light curve still exist. The phase reddening effect of asteroid spectra can also affect the classification, but its impact in the visible wavelength range is relatively small (Perna et al., 2018). At the same time, due to the significant differences in the reddening coefficients of different asteroids, it is difficult for us to normalize the observational results to zero phase angle. Overall, these errors may affect the accuracy of our classification of these NEAs. But considering that our purpose is to study the distribution of these objects by their taxonomic complex, the errors for individual objects can be neglected.

A number of surveys have been conducted to study the taxonomic

Table 2. Median orbital parameters (semi-major axis, eccentricity, inclination, perihelion, aphelion, and minimum orbital intersection distance) for the three major complexes considered in our analysis.

	a (au)	e	i (°)	q (au)	Q (au)	MOID (au)	T_J
C	1.54(0.56)	0.47(0.13)	10.6(6.5)	0.81(0.20)	2.11(0.83)	0.05(0.04)	6.2(2.5)
S	1.59(0.51)	0.48(0.09)	13.5(6.4)	0.91(0.20)	2.46(0.85)	0.10(0.07)	5.9(1.4)
X	1.93(0.49)	0.44(0.13)	10.1(6.0)	1.07(0.08)	2.77(1.16)	0.14(0.10)	5.2(1.9)

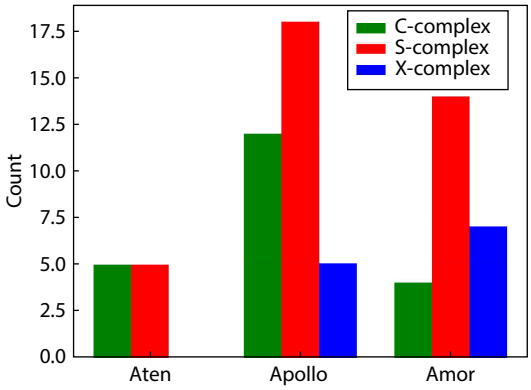

Figure 4. The distribution among three orbital types of the objects classified in our sample as belonging to the C-, S-, and X-complexes.

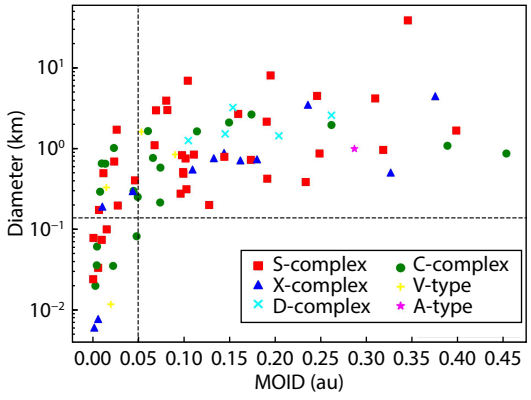

Figure 5. The Earth's MOID v.s. diameter in our sample. The vertical line at MOID = 0.05 au and the horizontal line at D = 140 m separate PHAs from the rest of the NEAs.

classification of NEAs in the recent years (e.g. Ieva et al., 2018, 2020; Lin CH et al., 2018; Hromakina et al., 2021). We compared the taxonomic distribution of the observed NEAs in our sample with those previous classifications. Since different studies may adopt different taxonomy, and the spectroscopic surveys can always classify the observed targets into subclasses, we re-counted their results following the taxonomy adopted in this work. As shown in Table 3, the percentage of C-complex NEAs in our work is close to the value (of about 22.6%) reported by Erasmus et al. (2017). However, this value is higher than the percentage (about 11%) found by Devogèle et al. (2019), and Hromakina et al. (2021). The percentage of S-complex NEAs varies from about 43.1% (Hromakina et al., 2021) to 67.7% (Lin CH et al., 2018; Popescu et al., 2019). The X-complex members represent 15.0% in our sample, which is close to the percentage reported by Perna et al. (2018) and Lin CH et al. (2018) but lower than the value in Hromakina et al. (2021). Such variation across the surveys may be caused by the different physical and orbital parameters of the observed targets, which is a result of the observational bias towards brighter objects.

Albedo values are available for 29 objects in our sample (e.g. Mainzer et al., 2011) and we used them to obtain additional confirmation of our classification. All three X-complex objects have low albedos that correspond to primitive P-type objects, following the Tholen taxonomy (Tholen, 1984).

Rabinowitz (1998) noted that reflectance colors of NEAs depend on their sizes and orbits. From the perspective of H, among bright asteroids (H < 17), the ratio of S-complex/C-complex is approximately 6:1, which aligns with findings from most literature listed in Table 3. However, for fainter asteroids (H > 17), the ratio n_S:n_C is about 3:4, showing a significant surplus of C-complex asteroids. Nevertheless, Luu and Jewitt (1989) proposed through simulations that observational selection effects caused an overrepresentation of S-complex asteroids. After bias correction, the ratio n_S:n_C was adjusted to the range of 0.8–1.9, consistent with the results of this study. Notably, when grouped by size, the ratios of S-complex/C-complex for diameters > 1 km and < 1 km asteroids (1.85 and 1.72, respectively) align well with the bias-corrected predictions of Luu and Jewitt (1989). Additionally, results in Figure 2 suggest that analyzing ratios of S-complex/C-complex based on diameter may hold greater statistical significance compared to analyses based on absolute magnitude. According to Binzel et al. (2019), based on a sample of more than 1000 NEOs, the distribution of taxonomic complexes remains stable in the 1–5 km size range. However, Hromakina et al. (2021) and Ieva et al. (2020) both find that there is a lower contribution of carbonaceous bodies below diameter < ~500 m, which could be due to observational bias.

DeMeo and Binzel (2008) and Simion et al. (2021) showed that most NEACOs have spectra properties similar to those of cometary nuclei, which indicates their possible cometary origin. As already mentioned, our sample has two objects with T_J < 2.8 and both have low albedo values that are consistent with inactive comets.

Table 3. The taxonomic distribution of different NEA samples observed by different methods.

	Method	NEA sample size	C-complex(%)	S-complex(%)	X-complex(%)
This work	Photometry	80	26.3	46.3	15.0
Erasmus et al. (2017)	Photometry	31	22.6	67.7	3.2
Perna et al. (2018)	Spectroscopy	147	9.6	65.3	17.8
Lin CH et al. (2018)	Photometry	92	6.5	63	13
Devogèle et al. (2019)	Spectroscopy	210	11.0	58.6	23.8
Popescu et al. (2019)	Spectroscopy	76	19.7	56.6	9.2
Ieva et al. (2018, 2020)	Photometry	1081	13	64	9
Hromakina et al. (2021)	Photometry	51	11.8	43.1	19.6

We explored potential connections between these NEAs with low T_J and small solar system bodies (SSSBs) in the outer solar system from two perspectives: color indices and source regions. First, from the color perspective, Jewitt et al. (2015) compiled color indices of various SSSBs in the outer solar system. We compared the average color indices of SSSBs with $2 < T_J < 3$ with our results and found that, within error margins, the colors of NEA (385268) are consistent with those of active Jupiter-family comets. Additionally, NEAs (417264) and 2012 FN62 exhibit colors that match, within uncertainties, those of defunct Short-period Nuclei. From the perspective of source regions, NEAs (385268) and 2012 FN62 have probabilities of 94% and 97%, respectively, of originating from Jupiter's 2:1 mean-motion resonance zone through the NEOMOD Simulator (Nesvorný et al., 2024). Hsieh et al. (2020) conducted numerical simulations of the dynamical evolution of Themis family asteroids in the main belt. They found that orbital eccentricities and inclinations of asteroids are excited under the influence of Jupiter's 2:1 mean-motion resonance, causing their orbits to gradually approach and cross those of major planets (particularly terrestrial planets, Jupiter, and Saturn). During close encounters with these planets, their T_J values may decrease to a range similar to that of Jupiter-family comets ($2 < T_J < 3$). Combining the results of color properties and source region analyses, we propose that NEA (385268) is likely to have originated as a Jupiter family comet, probably supplied by the Themis family through the Jupiter 2:1 mean-motion resonance.

NEAs with MOID values ≤ 0.05 au and diameter $D \leq 140$ m are classified as PHAs. These objects pass by the Earth so closely and are generally large enough that they have potential to cause an impact of regional-scale consequence. Among the PHAs analyzed by Ieva et al. (2020), the overall majority of them belong to the S-complex, while in our sample, the C- and S-complex share the same proportion. If there are more C-complex objects among PHAs than expected, planetary defense could be more challenging than previously thought, because the effect of orbit deflection using kinetic impact for porous objects is relatively low (Perna et al., 2013), and C-complex objects tend to be more porous than S-complex objects.

5. Conclusions

During the one-year multicolor photometric survey of NEAs, we obtained B-V-R-I color indices for 84 NEAs. Then we compared the color indices with reflectance sample spectra of each type from DeMeo et al. (2009) and derived a taxonomic classification for 80 NEAs. The overall majority in our sample belong to the S-complex (37 objects), while the C-, D- and X-complexes account for 21, 5, and 12 objects, respectively. The B-R versus V-I color diagram shows that the defined taxonomic complexes occupy different regions, and proves the reliability of our taxonomy.

The analysis of the size distribution among taxonomic complexes shows that C/X-complex asteroids are overrepresented among smaller objects ($H > 17.0$), with their fractional abundance nearly doubled compared to larger NEAs ($H \leq 17.0$). This aligns with previous studies, suggesting observational biases favoring brighter, higher-albedo S-complex asteroids in smaller size ranges. After applying albedo-based diameter corrections, the ratios of S-complex/C-complex for diameters >1 km (1.85) and <1 km (1.72) closely match the bias-corrected predictions of Luu and Jewitt (1989), implying that our observational strategy may inherently mitigate size-dependent biases.

The analysis of the orbital parameters of objects in our sample (a, q, Q, MOID, T_J) confirms that primitive C/D-complex NEAs have a dominant role in NEACOs, suggesting possible cometary origin. Notably, NEA (385268) exhibits spectral and dynamical properties consistent with Jupiter-family comets, likely originating from the Themis family via the 2:1 mean-motion resonance. X-complex asteroids show a preference for Amor-type orbits, while S-complex members are prevalent in both Apollo and Amor groups.

Among 13 potentially hazardous asteroids (PHAs) in our sample, C- and S-complexes are equally represented (5 each), suggesting that C-complex members may constitute a larger fraction of PHAs than previously thought. This raises concerns for planetary defense, as the porous structures of C-complex asteroids may reduce the effectiveness of kinetic impact deflection strategies (e.g., Stickle et al., 2022).

Future studies should expand taxonomic classification of NEAs and focus more on the primitive ones. We need to observe fainter bodies in order to improve our understanding of sub-kilometer NEAs. Future multi-color observations should broaden the wavelength range covered by filters, for instance, by incorporating the infrared z-band. This expansion will enhance classification accuracy and enable the acquisition of mineralogical information via the 1-micrometer silicate absorption band.

Acknowledgments

This research is funded by the China National Space Administration (KJSP2023020105). This research has been supported by the National Key R&D Program of China (Grant No.2023YFA1608100), the NSFC (Grant No.62227901) and the Minor Planet Foundation. This paper is also based on work supported by the Egyptian Science, Technology & Innovation Funding Authority (STDF) under Grant No.48102.

References

Azzam, Y. A., Elnagahy, F. I. Y., Ali, G. B., Essam, A., Saad, S., Ismail, H., Zead, I., Ahmed, N. M., Yoshida, M., … Mack, P. (2022). Kottamia Faint Imaging Spectro-Polarimeter (KFISP): Opto-mechanical design, software control and performance analysis. *Exp. Astron.*, *53*(1), 45–70. https://doi.org/10.1007/s10686-021-09802-z

Barbary, K. (2016). SEP: Source extractor as a library. *J. Open Source Softw.*, *1*(6), 58. https://doi.org/10.21105/joss.00058

Binzel, R. P., Morbidelli, A., Merouane, S., DeMeo, F. E., Birlan, M., Vernazza, P., Thomas, C. A., Rivkin, A. S., Bus, S. J., and Tokunaga, A. T. (2010). Earth encounters as the origin of fresh surfaces on near-Earth asteroids. *Nature*, *463*(7279), 331–334. https://doi.org/10.1038/nature08709

Binzel, R. P., DeMeo, F. E., Turtelboom, E. V., Bus, S. J., Tokunaga, A., Burbine, T. H., Lantz, C., Polishook, D., Carry, B., … Kohout, T. (2019). Compositional distributions and evolutionary processes for the near-Earth object population: Results from the MIT-Hawaii Near-Earth Object Spectroscopic Survey (MITHNEOS). *Icarus*, *324*, 41–76. https://doi.org/10.1016/j.icarus.2018.12.035

Bus, S. J., and Binzel, R. P. (2002). Phase II of the small main-belt asteroid spectroscopic survey: A feature-based taxonomy. *Icarus*, *158*(1), 146–177.

https://doi.org/10.1006/icar.2002.6856

DeMeo, F., and Binzel, R. P. (2008). Comets in the near-Earth object population. *Icarus*, *194*(2), 436–449. https://doi.org/10.1016/j.icarus.2007.10.011

DeMeo, F. E., Binzel, R. P., Slivan, S. M., and Bus, S. J. (2009). An extension of the Bus asteroid taxonomy into the near-infrared. *Icarus*, *202*(1), 160–180. https://doi.org/10.1016/j.icarus.2009.02.005

DeMeo, F. E., Binzel, R. P., and Lockhart, M. (2014). Mars encounters cause fresh surfaces on some near-Earth asteroids. *Icarus*, *227*, 112–122. https://doi.org/10.1016/j.icarus.2013.09.014

Devogèle, M., Moskovitz, N., Thirouin, A., Gustaffson, A., Magnuson, M., Thomas, C., Willman, M., Christensen, E., Person, M., … Skiff, B. (2019). Visible spectroscopy from the Mission Accessible Near-Earth Object Survey (MANOS): Taxonomic dependence on asteroid size. *Astron. J.*, *158*(5), 196. https://doi.org/10.3847/1538-3881/ab43dd

Erasmus, N., Mommert, M., Trilling, D. E., Sickafoose, A. A., van Gend, C., and Hora, J. L. (2017). Characterization of near-Earth asteroids using KMTNet-SAAO. *Astron. J.*, *154*(4), 162. https://doi.org/10.3847/1538-3881/aa88be

Ginsburg, A., Sipőcz, B. M., Brasseur, C. E., Cowperthwaite, P. S., Craig, M. W., Deil, C., Guillochon, J., Guzman, G., Liedtke, S., … The Astroquery Collaboration, a Subset of the Astropy Collaboration. (2019). astroquery: An astronomical web-querying package in Python. *Astron. J.*, *157*(3), 98. https://doi.org/10.3847/1538-3881/aafc33

Harris, A. W., and Harris, A. W. (1997). On the revision of radiometric albedos and diameters of asteroids. *Icarus*, *126*(2), 450–454. https://doi.org/10.1006/icar.1996.5664

Hasselmann, P. H., Fulchignoni, M., Carvano, J. M., Lazzaro, D., and Barucci, M. A. (2015). Characterizing spectral continuity in SDSS *u'g'r'i'z'* asteroid photometry. *Astron. Astrophys.*, *577*, A147. https://doi.org/10.1051/0004-6361/201424620

Hromakina, T., Birlan, M., Barucci, M. A., Fulchignoni, M., Colas, F., Fornasier, S., Merlin, F., Sonka, A., Petrescu, E., … The NEOROCKS Team. (2021). Photometric survey of 55 near-Earth asteroids. *Astron. Astrophys.*, *656*, A89. https://doi.org/10.1051/0004-6361/202141600

Hsieh, H. H., Novaković, B., Walsh, K. J., and Schörghofer, N. (2020). Potential Themis-family asteroid contribution to the Jupiter-family comet population. *Astron. J.*, *159*(4), 179. https://doi.org/10.3847/1538-3881/ab7899

Ieva, S., Dotto, E., Lazzaro, D., Perna, D., Fulvio, D., and Fulchignoni, M. (2016). Spectral characterization of V-type asteroids – II. A statistical analysis. *Mon. Not. R. Astron. Soc.*, *455*(3), 2871–2888. https://doi.org/10.1093/mnras/stv2510

Ieva, S., Dotto, E., Mazzotta Epifani, E., Perna, D., Rossi, A., Barucci, M. A., Di Paola, A., Speziali, R., Micheli, M., … Bertini, I. (2018). Photometric survey of 67 near-Earth objects. *Astron. Astrophys.*, *615*, A127. https://doi.org/10.1051/0004-6361/201732154

Ieva, S., Dotto, E., Mazzotta Epifani, E., Perna, D., Fanasca, C., Lazzarin, M., Bertini, I., Petropoulou, V., Rossi, A., … Perozzi, E. (2020). Extended photometric survey of near-Earth objects. *Astron. Astrophys.*, *644*, A23. https://doi.org/10.1051/0004-6361/202038968

Jewitt, D. (2015). Color systematics of comets and related bodies. *Astron. J.*, *150*, 201. https://doi.org/10.1088/0004-6256/150/6/201

Kosai, H. (1992). Short-period comets and Apollo-Amor-Aten type asteroids in view of Tisserand invariant. *Celest. Mech. Dyn. Astron.*, *54*(1), 237–240. https://doi.org/10.1007/BF00049556

Kresák, L. (1972). Jacobian integral as a classificational and evolutionary parameter of interplanetary bodies. *Bull. Astron. Inst. Czech.*, *23*(1), 1–34.

Kron, R. G. (1980). Photometry of a complete sample of faint galaxies. *Astrophys. J., Suppl. Ser.*, *43*, 305–325. https://doi.org/10.1086/190669

Lang, D., Hogg, D. W., Mierle, K., Blanton, M., and Roweis, S. (2010). Astrometry.net: Blind astrometric calibration of arbitrary astronomical images. *Astron. J.*, *139*(5), 1782–1800. https://doi.org/10.1088/0004-6256/139/5/1782

Lin, C. H., Ip, W. H., Lin, Z. Y., Cheng, Y. C., Lin, H. W., and Chang, C. K. (2018). Photometric survey and taxonomic identifications of 92 near-Earth asteroids. *Planet. Space Sci.*, *152*, 116–135. https://doi.org/10.1016/j.pss.2017.12.019

Luu, J., and Jewitt, D. (1989). On the relative numbers of C types and S types among Near-Earth Asteroids. *Astron. J.*, *98*, 1905. https://doi.org/10.1086/115267

Mainzer, A., Grav, T., Masiero, J., Hand, E., Bauer, J., Tholen, D., McMillan, R. S., Spahr, T., Cutri, R. M., … Maleszewski, C. (2011). NEOWISE studies of spectrophotometrically classified asteroids: Preliminary results. *Astrophys. J.*, *741*(2), 90. https://doi.org/10.1088/0004-637X/741/2/90

Marsset, M., DeMeo, F. E., Burt, B., Polishook, D., Binzel, R. P., Granvik, M., Vernazza, P., Carry, B., Bus, S. J., … Rivkin, A. S. (2022). The debiased compositional distribution of MITHNEOS: Global match between the near-Earth and main-belt asteroid populations, and excess of D-type near-Earth objects. *Astron. J.*, *163*(4), 165. https://doi.org/10.3847/1538-3881/ac532f

Nesvorný, D., Vokrouhlický, D., Shelly, F., Deienno, R., Bottke,W. F., Fuls, C., Jedicke, R., Naidu, S.,Chesley, S. R., … Delbo, M. (2024). NEOMOD 3: The debiased size distribution of near Earth objects. *Icarus*, *417*, 116110. https://doi.org/10.1016/j.icarus.2024.116110

Nichols, C. R. (1993). Volatile products from carbonaceous asteroids. In J. S. Lewis, et al. (Eds.), *Resources of Near-Earth Space* (pp. 543–568). Tucson: University of Arizona Press.

Perna, D., Barucci, M. A., and Fulchignoni, M. (2013). The near-Earth objects and their potential threat to our planet. *Astron. Astrophys. Rev.*, *21*(1), 65. https://doi.org/10.1007/s00159-013-0065-4

Perna, D., Barucci, M. A., Fulchignoni, M., Popescu, M., Belskaya, I., Fornasier, S., Doressoundiram, A., Lantz, C., and Merlin, F. (2018). A spectroscopic survey of the small near-Earth asteroid population: Peculiar taxonomic distribution and phase reddening. *Planet. Space Sci.*, *157*, 82–95. https://doi.org/10.1016/j.pss.2018.03.008

Popescu, M., Vaduvescu, O., De León, J., Gherase, R. M., Licandro, J., Boacă, I. L., Şonka, A. B., Ashley, R. P., Močnik, T., … Errmann, R. (2019). Near-Earth asteroids spectroscopic survey at *Isaac Newton* Telescope. *Astron. Astrophys.*, *627*, A124. https://doi.org/10.1051/0004-6361/201935006

Rabinowitz, D. L. (1998). Size and orbit dependent trends in the reflectance colors of Earth-approaching asteroids. *Icarus*, *134*(2), 342–346. https://doi.org/10.1006/icar.1998.5951

Reddy, V., Corre, L. L., Hicks, M., Lawrence, K., Buratti, B. J., Abell, P. A., Gaffey, M. J., and Hardersen, P. S. (2012). Composition of near-Earth Asteroid 2008 EV5: Potential target for robotic and human exploration. *Icarus*, *221*(2), 678–681. https://doi.org/10.1016/j.icarus.2012.08.035

Roh, D. G., Moon, H. K., Shin, M. S., and DeMeo, F. E. (2022). A new approach to feature-based asteroid taxonomy in 3D color space. I. SDSS photometric system. *Astron. Astrophys.*, *664*, A51. https://doi.org/10.1051/0004-6361/202039551

Sergeyev, A. V., and Carry, B. (2021). A million asteroid observations in the Sloan Digital Sky Survey. *Astron. Astrophys.*, *652*, A59. https://doi.org/10.1051/0004-6361/202140430

Simion, N. G., Popescu, M., Licandro, J., Vaduvescu, O., de León, J., and Gherase, R. M. (2021). Spectral properties of near-Earth objects with low-Jovian Tisserand invariant. *Mon. Not. R. Astron. Soc.*, *508*(1), 1128–1147. https://doi.org/10.1093/mnras/stab2561

Stickle, A. M., DeCoster, M. E., Burger, C., Caldwell, W. K., Graninger, D., Kumamoto, K. M., Luther, R., Ormö, J., Raducan, S., … Wünnemann, K. (2022). Effects of impact and target parameters on the results of a kinetic impactor: Predictions for the double asteroid redirection test (DART) mission. *Planet. Sci. J.*, *3*(11), 248. https://doi.org/10.3847/PSJ/ac91cc

Szabó, G. M., Ivezić, Ž., Jurić, M., Lupton, R., and Kiss, L. L. (2004). Colour variability of asteroids in the Sloan Digital Sky Survey Moving Object Catalog. *Mon. Not. R. Astron. Soc.*, *348*(3), 987–998. https://doi.org/10.1111/j.1365-2966.2004.07426.x

Tancredi, G. (2014). A criterion to classify asteroids and comets based on the orbital parameters. *Icarus*, *234*, 66–80. https://doi.org/10.1016/j.icarus.2014.02.013

Tholen, D. J. (1984). Asteroid taxonomy from cluster analysis of photometry [Ph. D. Thesis]. University of Arizona, Tucson, AZ, USA.

Thomas, C. A., Trilling, D. E., Emery, J. P., Mueller, M., Hora, J. L., Benner, L. A. M., Bhattacharya, B., Bottke, W. F., Chesley, S., … Stansberry, J. A. (2011). ExploreNEOs. V. Average albedo by taxonomic complex in the near-Earth

asteroid population. *Astron. J.*, *142*(3), 85. https://doi.org/10.1088/0004-6256/142/3/85

Thomas, C. A., Naidu, S. P., Scheirich, P., Moskovitz, N. A., Pravec, P., Chesley, S. R., Rivkin, A. S., Osip, D. J., Lister, T. A., … Agrusa, H. F. (2023). Orbital period change of Dimorphos due to the DART kinetic impact. *Nature*, *616*(7957), 448–451. https://doi.org/10.1038/s41586-023-05805-2

Tonry, J. L., Stubbs, C. W., Lykke, K. R., Doherty, P., Shivvers, I. S., Burgett, W. S., Chambers, K. C., Hodapp, K. W., Kaiser, N., … Wainscoat, R. J. (2012). The Pan-STARRS1 photometric system. *Astrophys. J.*, *750*(2), 99. https://doi.org/10.1088/0004-637X/750/2/99

Vernazza, P., Binzel, R. P., Thomas, C. A., DeMeo, F. E., Bus, S. J., Rivkin, A. S., and Tokunaga, A. T. (2008). Compositional differences between meteorites and near-Earth asteroids. *Nature*, *454*(7206), 858–860. https://doi.org/10.1038/nature07154

Vernazza, P., Binzel, R. P., Rossi, A., Fulchignoni, M., and Birlan, M. (2009). Solar wind as the origin of rapid reddening of asteroid surfaces. *Nature*, *458*(7241), 993–995. https://doi.org/10.1038/nature07956

Ye, Q. Z. (2011). *BVRI* photometry of 53 unusual asteroids. *Astron. J.*, *141*(2), 32. https://doi.org/10.1088/0004-6256/141/2/32

Zhang, T., Xu, K., and Ding, X. L. (2021). China's ambitions and challenges for asteroid–comet exploration. *Nat. Astron.*, *5*(8), 730–731. https://doi.org/10.1038/s41550-021-01418-9